NUCL SCI TECH (2019) 30:41
https://doi.org/10.1007/s41365-019-0573-7

TRISO fuel volume fraction and homogeneity: a nondestructive characterization

K. V. Vrinda Devi[1] · J. N. Dubey[1] · Jyoti Gupta[1] · I. H. Shaikh[1]

Received: 7 August 2018 / Revised: 17 September 2018 / Accepted: 19 September 2018 / Published online: 12 February 2019

Abstract A new nondestructive method to estimate the volume fraction and homogeneity of tristructural isotropic (TRISO)-coated fuel particles in fuel compacts designed for high-temperature reactors has been developed using image analysis of conventional X-radiographs. The method is demonstrated on surrogate fuel compacts containing TRISO-coated particles with kernels made of zirconium dioxide. The methodology incorporates a correction for superimposed images of TRISO particles such that a single X-ray image obtained in any one random orientation is sufficient to characterize the fuel compact in terms of volume fraction and homogeneity. The method is based on the virtual segregation of images of each particle inside the compact with the aid of a calibration standard.

Keywords TRISO · Volume fraction · Homogeneity · Radiography

1 Introduction

High-temperature reactor (HTR) technology, with its inherent safety characteristics, has potential to use high-temperature coolant applications that involve high-temperature and process heat such as the production of hydrogen from water [1, 2]. High-temperature gas reactor (HTGR) designs incorporate tristructural isotropic (TRISO) fuel particles either in pebble-bed reactor (PBR) design or in block design. TRISO fuels are designed to achieve high fuel burnup and high coolant temperature [3]. TRISO particles are dispersed in graphite pebbles in PBR design or compacted into a fuel compacts in the prismatic design. TRISO fuel consists of a fuel kernel at the center, typically composed of an oxide, carbide, or oxycarbide of uranium, plutonium, or thorium. The fuel kernel is coated with a porous carbon buffer layer fission gas buildup by providing void volume. This is followed by three additional layers of isotropic coating materials: an inner pyrolytic carbon (IPyC) layer, a silicon carbide (SiC) layer, and an outer pyrolytic carbon (OPyC) layer. The SiC layer acts as the primary containment of fission products, while the PyC coatings on either side of the SiC assists it in accommodating internal pressure [4, 5].

TRISO-coated particle-based fuel is being considered for the future HTR of India [6, 7]. The TRISO fuel fabrication process starts by synthesizing fuel kernels through sol–gel process followed by multiple steps of chemical vapor deposition (CVD) to obtain the TRISO coating [8]. The coated particles are compacted in graphite matrix to produce fuel compacts, which are loaded into graphite fuel tubes. A schematic of the fuel particle showing the details of each layer of coating is given in Fig. 1.

Quality control in TRISO fuel fabrication requires extensive inspections for various fuel characteristics, and the development of new quality control techniques in accordance with fuel specifications is an important part of fuel technology development [9]. The volume fraction of TRISO particles is an important specification to ensure the required fissile content of the fuel as well as the homogeneous distribution of particles in fuel compacts. Techniques based on the analysis of X-radiographic images have been reported to ensure the homogeneity of fuel particle

✉ K. V. Vrinda Devi
kvvdevi@barc.gov.in

[1] Radiometallurgy Division, Bhabha Atomic Research Centre, Mumbai, India

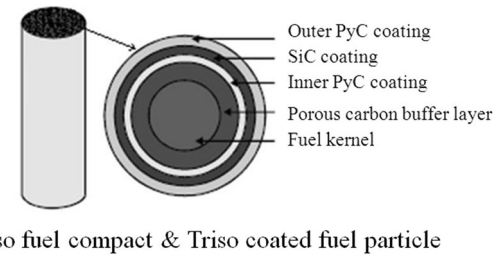

Fig. 1 Schematic of a typical TRISO-coated fuel particle and fuel compact

distribution inside the compact [10]. The gross evaluation of the volume fraction of particles in the compact was previously demonstrated using image analysis of X-radiographs, which incurred errors owing to the superimposition of images of particles in the compact [11]. X-ray tomography-based 3D mapping of TRISO particles has been studied for qualification of HTR pebbles with 60 mm diameter for fuel distribution [12]. This highly accurate technique used 720 X-ray images of the pebble obtained at 0.5° intervals for reconstruction of tomographic image by software. A simple nondestructive technique, which can be used for regular quality control inspection during bulk fabrication of TRISO fuel, was developed through the analysis of a single X-radiographic image obtained by the conventional film radiography method. A new analysis methodology was developed for accurate estimation of the volume fraction of TRISO fuel particles in fuel compacts using image analysis of conventional X-radiographic images. The novel method performs virtual segregation of overlapping radiographic images of each particle within the fuel compacts and estimates the total number of TRISO fuel particles loaded in each compact with high accuracy. The method can also be applied to verify the homogeneity of particle distribution. Details of the experiments and analysis carried out on TRISO particles and compacts synthesized using surrogate material, i.e., zirconium dioxide, for developing and validating the methodology are described.

2 Methodology

Conventional X-ray radiography carried out on the fuel compact provides a two-dimensional projected image of the fuel particles present inside the compact. The attenuation offered by the kernels of TRISO particles (zirconia in this study) is much higher compared that by the coating layers (mainly carbon) owing to the significantly higher mass number of the elements; hence, the kernels will only be clearly revealed in the X-radiographic image. The maximum possible thickness of the surrogate material resulting from the probable diametrical overlapping of particles may be considered as the object thickness for radiography. The diameters of the particle and compact along with the expected volume fraction could provide this information. By choosing the suitable X-ray energy that ensures full penetration, the images of all the particles inside the compact with or without superimposition may be obtained. Gray levels corresponding to the image of the surrogate material with different thicknesses may be identified using a calibration standard made using the same material as that of the TRISO kernel.

Since conventional X-radiography obtains a two-dimensional image of a three-dimensional object projected onto a plane (film/detector), it can result in partial or sometimes complete superimposition of the projected images of TRISO particles present inside the compact, as illustrated in Fig. 2. Hence, it is necessary to virtually segregate the individual images of each particle from the superimposed image in order to accurately estimate the number of fuel particles forming the complex image. The task of virtually segregating the images of TRISO particles inside the fuel compact can be performed by identifying the gray-level values in the complex image corresponding to each thickness of the material (zirconia) and probabilistically estimating the number of particles which could result in that thickness by virtue of diametrical superimposition inside the compact. Hence, the new analysis method was developed based on the virtual segregation of images from a complex image and probabilistic estimation of the formation of the corresponding thickness of the material.

The methodology adapted for virtual segregation of the radiographic images of TRISO particles is illustrated with a simple simulated representation of images of four particles in Fig. 3. In this example, the overlapping of images of particles 1 and 2 was 100%, but the images of particles 3 and 4 did not overlap with each other or any other image upon X-projection.

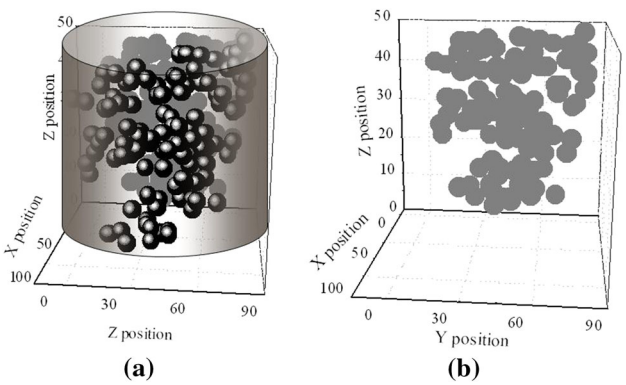

Fig. 2 **a** TRISO fuel compact along with its simulated radiographic image and **b** the simulated radiographic image

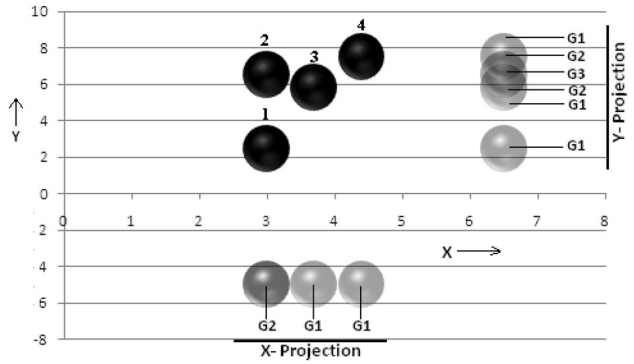

Fig. 3 Virtual segregation of projected images through gray-level segregation

Upon Y-projection, the image of particle 1 did not overlap with any other image, whereas the images of particles 2, 3, and 4 were superimposed on each other. The different levels of darkness in the resultant image may be divided into three classes: *G*1, *G*2, and *G*3, corresponding to the shadows of one particle, two particles, and three particles, respectively. The areas of portions of the image with gray levels *G*1, *G*2, and *G*3 may be estimated as *A*1, *A*2, and *A*3, respectively, using the image analysis software.

In the Y-projection of images in the example shown in Fig. 3, the estimated areas corresponding to gray levels *G*1, *G*2, and *G*3 are 190%, 75%, and 20%, respectively, of the area of an individual particle. Direct estimation of the number of particles corresponding to these areas was performed by dividing these areas by that of an individual particle. In this example, the values of *N*1, *N*2, and *N*3 are 1.9, 0.75, and 0.2, respectively. Since it is known that gray-level *G*1 corresponds to the attenuation offered by one particle, *G*2 by two particles, and *G*3 by three particles, the numbers were further multiplied by the corresponding contributing numbers (weightage values), i.e., *N*1 by 1, *N*2 by 2, and so on, to obtain the actual numbers. When multiplied with their weightage values, *N*1, *N*2, and *N*3 are 1.9, 1.5, and 0.6, respectively, the sum of which is 4. In the X-projection of this example, there are only two gray levels: *G*2 due to complete overlapping of two images, and *G*1 due to the un-overlapped individual images. *A*1 will be 200% of the area of an individual particle image resulting from two un-overlapped images, and *A*2 will have the same area as that of a single particle owing to the exact superimposition of images of two particles. The directly estimated numbers corresponding to *A*1 and *A*2 will be 1 and 2, respectively; when weighed, it will result in 2 and 2, the sum of which is 4. Since the images contributed by each of the particles are virtually segregated, the estimation does not depend on the orientation from which the radiograph is obtained; one single radiograph obtained in any random orientation will be sufficient for the estimation. The same algorithm can be applied to different segments of the compact radiograph of equal width in order to estimate the number of particles present in each segment which, in turn, estimates the homogeneity of the particle distribution inside the compact.

The probabilities of each gray level were also incorporated into the algorithm by considering the possible permutations of overlapping to estimate the segregated number of particles in the image with improved accuracy. The possible formation of each thickness equal to that of each step available in the step variation standard was estimated, as summarized in Table 1. A ZrO_2 thickness of 2.5 mm can only be obtained by complete overlapping of five kernels, whereas a thickness of 0.5 mm can be obtained either by a single particle or partial minimal overlapping of 2, 3, 4, or 5 particles, and so on. A minimum contribution of 0.1 mm was assumed from every single particle for the purpose of simplifying and categorizing the gray levels into only five classes. It was assumed that occurrence of each of these cases was equally probable or random. Hence, the areas corresponding to the gray levels owing to each step thickness were distributed with equal probability to all the possible occurrences mentioned in Table 1 as follows.

For example, in case 5, one-fifth of *A*1, which is the area of the portion with gray level *G*1 corresponding to the thickness of one particle (0.5 mm thick), was considered as *A*5, one-fifth as *A*4, one-fifth as *A*3, one-fifth as *A*2, and the remaining one-fifth as *A*1, assuming that a minimum thickness of 0.5 mm can be obtained from all the five possibilities with equal probability. The areas corresponding to all other gray levels were also treated in a similar manner in accordance with probabilities listed in Table 1. The effective areas (Ai_{eff}) corresponding to each of the areas (*A*1, *A*2, *A*3, *A*4, and *A*5) after this probabilistic distribution are calculated using Eqs. (1)–(5) for the final estimation.

$$A1_{\text{eff}} = A1/5 \tag{1}$$

$$A2_{\text{eff}} = A1/5 + A2/4 \tag{2}$$

$$A3_{\text{eff}} = A1/5 + A2/4 + A3/3 \tag{3}$$

$$A4_{\text{eff}} = A1/5 + A2/4 + A3/3 + A4/2 \tag{4}$$

$$A5_{\text{eff}} = A1/5 + A2/4 + A3/3 + A4/2 + A5 \tag{5}$$

The projected area of the image of an individual particle was estimated from the same image to avoid errors from image magnification. By dividing each of these effective area values by the area of a single particle, the number of images contributing to each gray value (*G*1, *G*2, and *G*3) in the final image can be directly estimated as *N*1, *N*2, and *N*3, respectively. Since it is known that *G*1 is caused by the

Table 1 Probability of different cases of particle overlapping

Case nos.	Thickness of ZrO_2 (mm)	Gray level	Possible number of contributing particles	Probability for each case
1	0.5	*G*1	1,2,3,4,5	1/5
2	1	*G*2	2,3,4,5	1/4
3	1.5	*G*3	3,4,5	1/3
4	2	*G*4	4,5	1/2
5	2.5	*G*5	5	1

thickness of one particle, *G*2 by the thickness of two particles, and so on, the directly estimated image numbers *N*1, *N*2, and *N*3 were converted into the number of particles forming the image by multiplying them with the corresponding weightage values of 1, 2, 3, etc., respectively. Their sum will provide the total number of particles that actually compose the final resultant image incorporating the superimposed images. With prior knowledge of the average particle size and the dimensions of the compact, the volume fraction of particles inside the compact can be estimated using the total number of particles.

3 Experimental

The surrogate kernels made of zirconia were synthesized through sol–gel route and TRISO coatings by successive CVD processes. Fuel compacts were fabricated by hot compaction of TRISO fuel particles after overcoating them with graphite. The compacts were fabricated by mixing the particles with graphite and phenolic resin, followed by compacting and sintering at 1750 °C. A fraction of TRISO particles was kept at 25% of the die volume during the synthesis of compacts.

The coated surrogate TRISO particles were inspected for their distribution in terms of geometric aspects such as diameter, sphericity, and aspect ratio. Cross-sectional surface preparations were carried out on samples to review the different coating layers of TRISO particles and measure the average kernel diameter, which was found to be $\sim$ 500 µm. The sintered compacts were synthesized with a diameter of 10 mm and height of 35 mm (Fig. 4).

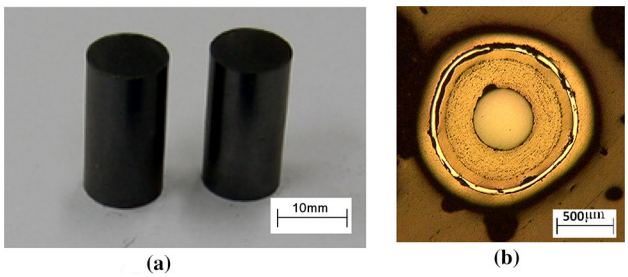

Fig. 4 **a** Photograph of the experimental compacts and **b** cross-sectional microscopic view of the TRISO-coated particle (color online)

Although weighing and calculation methods, which are suggested for inspecting the volume fraction of fuel particles in the compacts, revealed approximately the same volume fraction, it was not possible to understand the distribution of particles inside the compact by these methods. A compact, which showed some visibly "empty" edge and corner portions in the radiographic image and thus expected to have heterogeneous fuel particle distribution, was chosen for the analysis so that the results can be correlated with the image more clearly.

Diametrical overlap of a maximum of five particles was visualized by considering the limiting factors: compact diameter and volume fraction occupied by particles. A thickness variation standard was fabricated in-house based on the aforementioned methodology. The objective is to generate five different gray levels corresponding to the superimposition of radiographic images of different material thicknesses resulting from varying numbers of TRISO particles. The standard was fabricated by vertically stacking TRISO particles in increasing numbers with a step variation of one and then fixing them in place using glue. Hence, there were vertical stacks of 2, 3, 4, and 5 particles placed along with a single particle for comparison. It is important to use TRISO particles of the same composition and density as that used in the compact for the thickness variation standard.

Since the atomic number of zirconium is much higher than that of carbon, the images will be formed by the kernels rather than the surrounding coating layers. The mass attenuation coefficients of zirconium and carbon (graphite matrix) were compared at different X-ray energies and varying thicknesses of zirconium [13]. It was observed that the correlation between the attenuating material thickness and the ratio I/I_0 can be considered linear with a considerable slope at 100 keV for the thickness range of 0.05–0.25 cm, which is the region of interest. The slope of the correlation was lower beyond this energy, which can reduce the contrast between the images of each

standard stack. X-ray energies approximately within the range of 80–100 keV were chosen for radiography by considering the 100 kV potential on the X-ray tube.

The correlation (Fig. 5) was extended to the thickness range of interest according to the fuel compact dimensions and X-ray energy chosen to ensure linearity. However, extending these to very large dimensions could result in low-contrast images and subsequently reduce the accuracy of analysis results.

Image analysis of the step variation standard made of TRISO particles with zirconia kernel was first carried out to validate the algorithm for virtual segregation of overlapping radiographic images [14]. The radiographs of the fuel compacts were obtained under the same conditions as that of the step variation standard to ensure the equivalence of the imaging process.

The thickness standard made using the TRISO particle stacks was placed on the film cassette with the aid of a holder to generate the five possible complete overlapping conditions of the particles during imaging. X-radiographs of this standard were acquired with X-ray exposure of 90 kV, 4 mA, and 2 min from a YXLON X-ray machine using D4 Agfa film. The films were processed through the standard process, and radiographs were digitized using a radiograph (film) scanner (Epson V600) with a resolution of 2400 dpi. The digital images were analyzed using image analysis software (Metal power image analyzer version 3.0.0.9 by Metal Power India (Pvt.) Ltd.) to identify the different gray levels corresponding to each of the particle stacks.

The schematic radiography configuration of the thickness standard is shown in Fig. 6a along with its radiograph in Fig. 6b with the corresponding numbers marked in each image. The binary image of the radiograph obtained through the image analysis software is shown in Fig. 6c. The image was suitably thresholded into the five different gray levels in order to obtain the gray levels corresponding to particles overlapping from 1 to 5 in number. The same thresholding was applied to the fuel compact for the analysis of gray levels (Fig. 7).

The algorithm described above was applied to the digital radiographic image of the compact to estimate the average volume fraction of TRISO particles, and to approximately equal-sized segments of the same image for homogeneity analysis; the results are discussed below.

4 Results and discussion

The geometric aspects of the particles were measured statistically, and the average values as well as range were found to be within the specified limits. The diameter of the

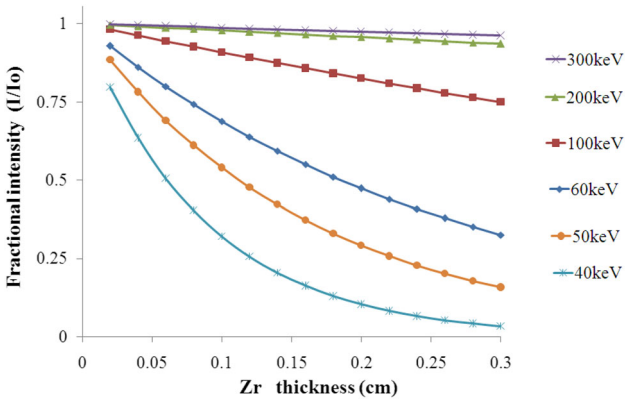

Fig. 5 Fractional intensity (I/I_0) offered by varying thicknesses of Zr to different energies of X-rays (color online)

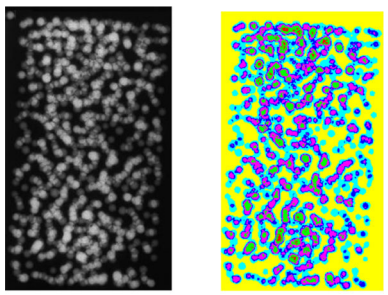

Fig. 7 X-ray image of the fuel compact acquired under the same conditions is shown in (**a**) and its thresholded image in (**b**) (color online)

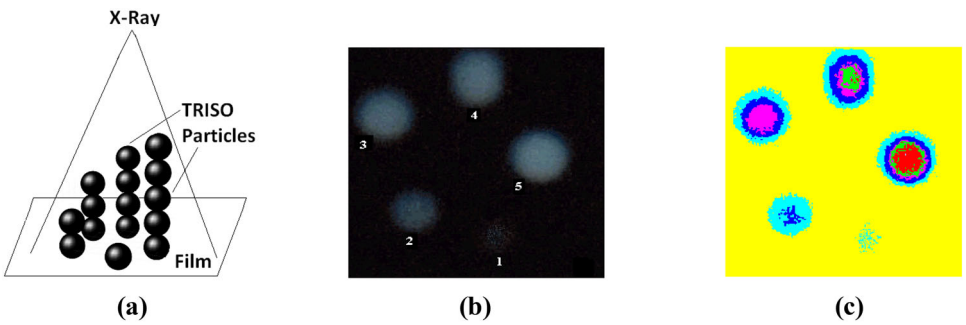

Fig. 6 **a** Schematic of the thickness standard and radiographic setup, **b** radiograph of thickness variation standard, and **c** the gray-level thresholded and color-coded image (color online)

particles ranged between 1.005 and 1.089 mm, and their sphericity varied from 0.92 to 1.09. The average volume of a TRISO particle estimated by geometric calculation was 0.536 mm^3. The measurements were taken using a profile projector on 100 particles to obtain the statistical values. The average diameter of the kernel was considered to be 0.5 mm. These characteristics were used for the volume calculation of the TRISO particle.

The areas of portions of the image having each of these gray levels were obtained by area fraction analysis of the thresholded image using the image analysis software. The algorithm based on gray-level identification for virtual segregation was validated based on the thickness standard and found to have 87% accuracy in predicting the number of particles [14]. This algorithm was modified to improve the accuracy up to 98% by including the probabilities of overlapping and applied to the fuel compact as shown in Table 1; estimation was carried out as explained below (Table 2).

Area fractions of the total frame area corresponding to portions with gray levels *G*1, *G*2, *G*3, *G*4, and *G*5 were obtained from the image analysis and termed as *A*1, *A*2, *A*3, *A*4, and *A*5, respectively, as shown in Fig. 8.

The image of the fuel compact was divided into eight segments, and the same algorithm was applied to each segment. The results of the analysis are summarized in Table 3. It can be seen that the compact had heterogeneous distribution of fuel particles with volume fractions ranging from 18.63 to 27.11%. The top portion of the compact visibly had an empty portion where no particles were seen in the radiograph, which resulted in lower volume fraction in the first segment. The accuracy of estimation of number of particles was 90% when applied to the full compact, more than 99% when applied to individual strips of images and summed up.

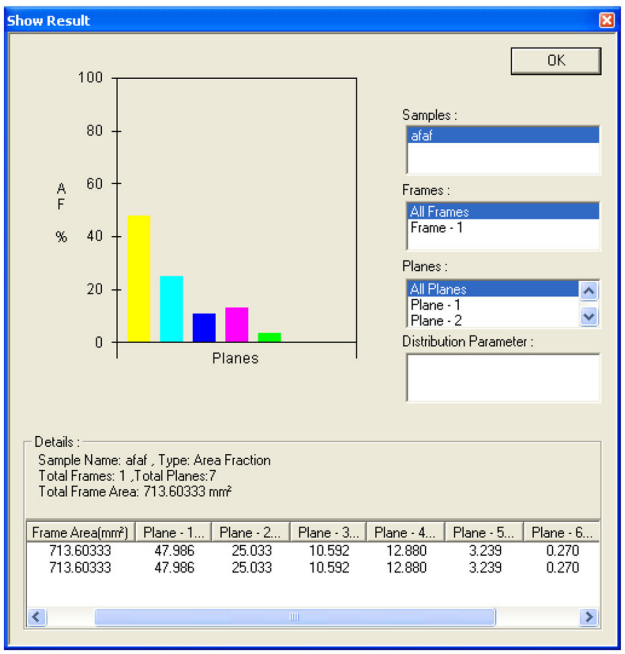

Fig. 8 Screenshot of the area fraction analysis result (color online)

Table 3 Result of homogeneity analysis

Segment number	Segment height (mm)	Volume fraction (%)
1	3.36	18.63
2	4.46	27.11
3	4.18	25.29
4	4.6	26.55
5	4.7	25.91
6	4.65	24.15
7	4.45	26.55
8	4.6	25.57

Table 2 Actual calculations for the fuel compact using the algorithm

Gray level	Matrix	*G*1	*G*2	*G*3	*G*4	*G*5	Total
Area % (from Fig. 7)	47.99	25.03	10.59	12.88	3.24	0.27	100
A_{actual} (mm^2)	342.43	178.64	75.58	91.91	23.11	1.93	713.60
A_{eff} (mm^2)		35.73	54.62	85.26	96.82	98.74	
Area of single kernel image (*a*) (mm^2)		0.9 (from the same image of the compact)					
Number of particles $N = (A_{eff}/a)$		39.69678	60.69247	94.73384	107.5747	109.7155	412.4132
Number weightage factor (*n*)		1	2	3	4	5	
Actual number ($N * n$)		39.69678	121.3849	284.2015	430.2987	548.5774	1424.159
Volume of single particle (mm^3)		0.536					
Volume of total number of particles (mm^3)		745.31					
Compact volume (mm^3)		2747.5					
Volume fraction (%)		27.12					

5 Conclusion

The newly developed methodology was found to be effective in estimating the volume fraction of TRISO fuel particles with surrogate material (zirconium dioxide kernels) in compacts with 99% accuracy. Since the method is independent of radiograph orientation, a single radiographic image obtained in any random direction will be sufficient for the analysis; hence, the method can be employed in fuel characterization during regular fabrication which involves a very large number of compacts. As a nondestructive, fast, and easy-to-use method, it is possible to apply this technique to all fuel compacts, which makes the average results of volume fraction and homogeneity highly reliable. The optimization of radiographic parameters can be carried out for actual fuel materials based on this study by appropriately increasing the X-ray energy to ensure complete penetration.

Acknowledgements The authors express their sincere gratitude to Shri Vivek Bhasin, Associate Director, NFG, BARC for their valuable support. Valuable inputs from Shri P. S. Kutty and Shri D. M. Mohod Retd. Officers, Radiometallurgy division, BARC, are gratefully acknowledged.

References

1. H. Nickel, K. Hofmann, W. Wachholz et al., The helium-cooled high-temperature reactor in the Federal Republic of Germany safety features, integrity concept, outlook for design codes and licensing procedures. Nucl. Eng. Des. **127**, 181–190 (1991). https://doi.org/10.1016/0029-5493(91)90015-a
2. E. Teuchert, R.B. Rossa, K.A. Haas et al., Physics features of the HTR for process heat. Nucl. Eng. Des. **78**(2), 147–154 (1984). https://doi.org/10.1016/0029-5493(84),90300-5
3. R.E. Bullock, Design of coated fuel particles for a hybrid fusion–fission system. Nucl. Eng. Des. **61**, 331–345 (1980). https://doi.org/10.1016/0029-5493(80),90005-9
4. IAEA-TECDOC-1645, *High Temperature Gas Cooled Reactor Fuels and Materials* (2010) ISBN: 978-92-0-153110-2
5. K. Sawa, T. Tobita, H. Mogi et al., Fabrication of the first-loading fuel of the high temperature engineering test reactor. J. Nucl. Sci. Technol. **36**, 683–690 (1999). https://doi.org/10.1080/18811248.1999.9726255
6. I.V. Dulera, R.K. Sinha, High temperature reactors. J. Nucl. Mater. **383**, 183–188 (2008). https://doi.org/10.1016/j.jnucmat.2008.08.056
7. R.K. Sinha, I.V. Dulera, Carbon based materials—applications in high temperature nuclear reactors. Ind. J. Eng. Mat. Sci. **17**, 321–326 (2010)
8. R.V. Pai, P.K. Mollick, A. Kumar et al., Recovery and recycling of uranium from rejected coated particles for compact high temperature reactors. J. Nucl. Mater. **473**, 229–236 (2016). https://doi.org/10.1016/j.jnucmat.2016.02.030
9. K. Sawa, S. Suzuki, S. Shiozawa et al., Safety criteria and quality control of HTTR fuel. Nucl. Eng. Des. **208**, 305–313 (2001). https://doi.org/10.1016/s0029-5493(01)00358-2
10. F. Charollais, C. Perrais, D. Moulinier et al., Latest achievements of CEA and AREVA NP on HTR fuel fabrication. Nucl. Eng. Des. **238**, 2854–2860 (2008). https://doi.org/10.1016/j.nucengdes.2008.01.020
11. J.N. Dubey, B.P. Patil, D.M. Mohod et al., A technique for gross evaluation of TRISO coated particle distribution in fuel compacts for CHTR-CF, in *Proceedings of International Conference on Character Quality Control Nuclear Fuels (CQCNF)* 152 (2012). www.inis.iaea.org/search/search.aspx?origq=RN:43034450
12. P.R. Hania, B. Janssen, A.V. Fedorov et al., Qualification of HTR pebbles by X-ray tomography and thermal analysis. Nucl. Eng. Des. **251**, 47–52 (2012). https://doi.org/10.1016/j.nucengdes.2011.11.036
13. J.H. Hubbell, S.M. Seltzer, Tables of X-ray mass attenuation coefficients and mass energy-absorption coefficients from 1 keV to 20 MeV for elements Z = 1 to 92 and 48 additional substances of dosimetric interest, (version 1.4) [Online] National Institute of Standards and Technology, Gaithersburg. https://dx.doi.org/10.18434/T4D01F
14. K.V. Vrinda Devi, J. Gupta, J.N. Dubey et al., Image analysis for virtual segregation of overlapped radiographic images. e-J. Nondestr. Test. NDT.net issue 20(6) (2015). ISSN: 1435-4934 www.ndt.net/?id=17832